Electronic Interaction between Nitrogen Atoms in Doped Graphene

Yann Tison,[*,†,⊥] Jérôme Lagoute,[*,†] Vincent Repain,[†] Cyril Chacon,[†] Yann Girard,[†] Sylvie Rousset,[†] Frédéric Joucken,[‡] Dimpy Sharma,[‡] Luc Henrard,[‡] Hakim Amara,[§] Ahmed Ghedjatti,[§] and François Ducastelle[§]

[†]Laboratoire Matériaux et Phénomènes Quantiques, CNRS-Université Paris 7, 10 Rue Alice Domon et Léonie Duquet, 75205 Paris Cedex 13, France, [‡]Department of Physics, University of Namur, Rue de Bruxelles 61, B-5000 Namur, Belgium, and [§]Laboratoire d'Etude des Microstructures, ONERA-CNRS, BP 72, 92322 Châtillon Cedex, France [⊥]Present address: Université de Pau et des Pays de l'Adour, IPREM - ECP CNRS UMR 5254, Hélioparc Pau-Pyrénées, 2 Avenue du Président Angot, 64053 Pau Cedex 9, France.

ABSTRACT Many potential applications of graphene require either the possibility of tuning its electronic structure or the addition of reactive sites on its chemically inert basal plane. Among the various strategies proposed to reach these objectives, nitrogen doping, *i.e.*, the incorporation of nitrogen atoms in the carbon lattice, leads in most cases to a globally n-doped material and to the presence of various types of point defects. In this context, the interactions between chemical dopants in graphene have important consequences on the electronic properties of the systems and cannot be neglected when interpreting spectroscopic data or setting up devices. In this report, the structural and electronic properties of complex doping sites in nitrogen-doped graphene have been investigated by means of scanning tunneling microscopy and spectroscopy, supported by density functional theory and tight-binding calculations. In particular, based on combined experimental and simulation works, we have systematically studied the electronic fingerprints of complex doping configurations made of pairs of substitutional nitrogen atoms. Localized bonding states are observed between the Dirac point and the Fermi level in contrast with the unoccupied state associated with single substitutional N atoms. For pyridinic nitrogen sites (*i.e.*, the combination of N atoms with vacancies), a resonant state is observed close to the Dirac energy. This insight into the modifications of electronic structure induced by nitrogen doping in graphene provides us with a fair understanding of complex doping configurations in graphene, as it appears in real samples.

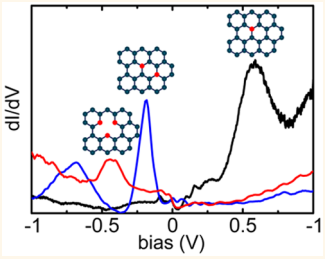

KEYWORDS: graphene · nitrogen doping · STM · STS · DFT · tight-binding

Doping or functionalizing graphene is a key method to develop carbon-based electronics or other applications taking advantage of the properties of this 2D material.[1] Several strategies are employed in order to dope graphene. A first approach is to apply a bias voltage between a graphene sheet and a gate in a graphene flake device,[2] the sign of this bias resulting in either p- or n-doping. A second method involves the reversible adsorption of inorganic molecules such as NO_2[3] or organic molecules, for example, toluene[4] or triazine.[5] The preceding methods are reversible, which is well adapted to some applications but not to those requiring stable changes of electronic structure. A route to permanent modification is to substitute foreign atoms such as boron[6] or nitrogen[6,7] for carbon, allowing a fine-tuning of the electronic band structure of graphene while avoiding strong relaxation effects.[8−11]

In recent years, boron- and nitrogen-doped graphene has successfully been implemented into electronic devices such as transistors[12] or gas sensors.[13] Moreover, the potential use of the foreign atoms in these materials as catalytic sites has been demonstrated by several investigations.[14−16] Nitrogen doping has been achieved either directly during the synthesis by CVD[8,11,17,18] or in a postsynthesis irradiation[19] or by N_2-plasma treatment[9] (see also refs 7, 20−23). These approaches mostly lead to single nitrogen atoms substituted for carbon atoms, associated with the presence of a donor state[9] and thus with n-type doping. However, other more complex configurations have been observed in scanning tunneling microscopy (STM) measurements.[8,9,24] In particular, Lv *et al.* propose attributing the majority of the defects observed after the growth of N-doped graphene at ambient pressure to second neighbor pairs of nitrogen atoms.[18]

* E-mail: yann.tison@univ-pau.fr.
* E-mail: jerome.lagoute@univ-paris-diderot.fr.

Received for review October 24, 2014 and accepted January 5, 2015.

Published online January 05, 2015
10.1021/nn506074u

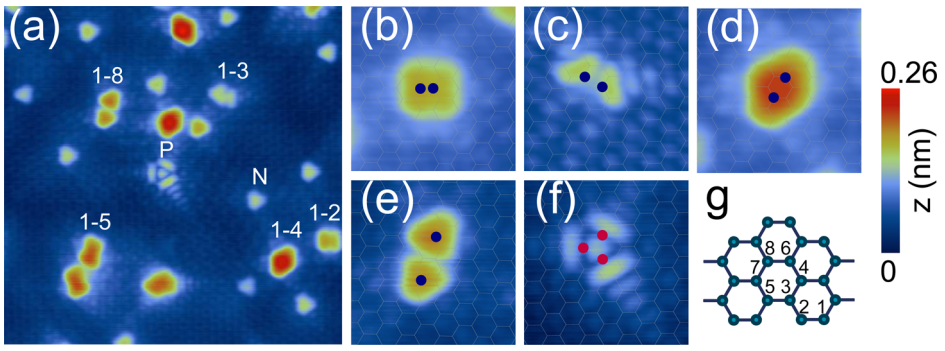

Figure 1. (a) STM image (−0.5 V, 400 pA, 10 × 10 nm^2) of a nitrogen-doped graphene showing various nitrogen configurations; zoomed STM images of (b) a 1−2 nitrogen pair, (c) a 1−3 nitrogen pair, (d) a 1−4 nitrogen pair, (e) a 1−8 nitrogen pair, (f) a triangular shape labeled P; the color scale used for the 10 × 10 nm^2 image and for the zooms is shown on the right; (g) labels used for the nitrogen pairs. A single substitutional nitrogen atom is labeled N in panel (a).

It has been shown that, for isolated substitutional N atoms, scanning tunneling spectroscopy (STS) reveals a localized resonant unoccupied electronic state, about 0.5 eV above the Fermi level for 0.6% nitrogen doping.[9,25] The identification of more complex doping sites and their respective electronic properties has barely been discussed so far, although they correspond to a non-negligeable amount of the doping sites. In particular, understanding the nitrogen−nitrogen interaction in graphene is mandatory to master the properties of doped graphene. Furthermore, as illustrated by density functional theory (DFT) calculations that show different binding energies for adsorbed gas molecules on various boron or nitrogen sites,[26] a more detailed description of the geometrical and electronic properties of the various structures induced by nitrogen incorporation in graphene is a necessary step toward the understanding of the adsorption of reactive species on a N-doped graphene.

In this paper, we report on the identification of complex configurations observed in the STM images of a few-layer graphene sample, grown on SiC(000$\bar{1}$) and treated with a remote N_2 plasma,[9] with a strong focus on nitrogen pairs and pyridinic nitrogen sites. We show that an occupied localized state is formed on the pairs between the Fermi level and the Dirac energy. For pyridinic nitrogen a peak at the Dirac energy is observed as previously predicted.[27] Our interpretations are supported by tight-binding (TB) and DFT calculations. Particular attention is paid to the spatial localization of the resonant states and to the resulting consequences for STS/STM fingerprints of complex nitrogen doping.

RESULTS AND DISCUSSION

Experiments. In this study, we used graphene samples grown on the C-terminated 6H-SiC (000$\bar{1}$) surface. These samples consist of more than five graphene layers electronically decoupled from each other thanks to rotational disorder.[9] Hence, the top layer is not affected by any charge transfer from the substrate,[28−35] which is crucial for investigating the band structure modifications induced by the introduction of nitrogen atoms. Reference nondoped samples, prepared in the conditions used for the doped sample studied here, have been characterized using STM/STS, and the results have been presented elsewhere.[9,36] The STM images obtained for these reference samples display large domains for which the honeycomb lattice of graphene is seen[9] and separated by grain boundaries.[36] The STS spectra obtained for these nondoped samples show that the Dirac point is found at the Fermi energy.[36]

After postsynthesis doping, in addition to the honeycomb lattice of graphene with an interatomic distance of 1.4 Å, the graphene samples show several types of point defects, as illustrated by the STM image in Figure 1a. As already discussed,[9] the majority of the nitrogen-related defects appear as globally triangular structures, which have been identified as the signature of single substitutional nitrogen atoms. This shape is due to a local redistribution of density of states from the nitrogen atoms to their first carbon neighbors.[8,9] Furthermore, it has been shown that the resulting STM pattern can be affected by experimental parameters such as the sample bias[9] or the chemical nature of the tip apex.[24] The STM image shows two possible orientations in similar proportions for these triangles, which indicates that the nitrogen dopants can occupy either sublattice of the graphene after our postsynthesis doping process. This result contrasts with the sublattice segregation reported in samples doped during the growth.[11] Since theoretical investigations have recently shown that the presence of point defects on only one graphene sublattice can lead to a gap opening,[25,37] this discrepancy may lead to different behaviors in terms of transport. This illustrates the interest in investigating the doping effects in 2D structures such as graphene as well as the parameters governing the distribution of N atoms on either a single or both graphene sublattices.

In Figure 1a, other atomic-scale defects are observed with different shapes. Some of them can easily be recognized as the combination of two triangular

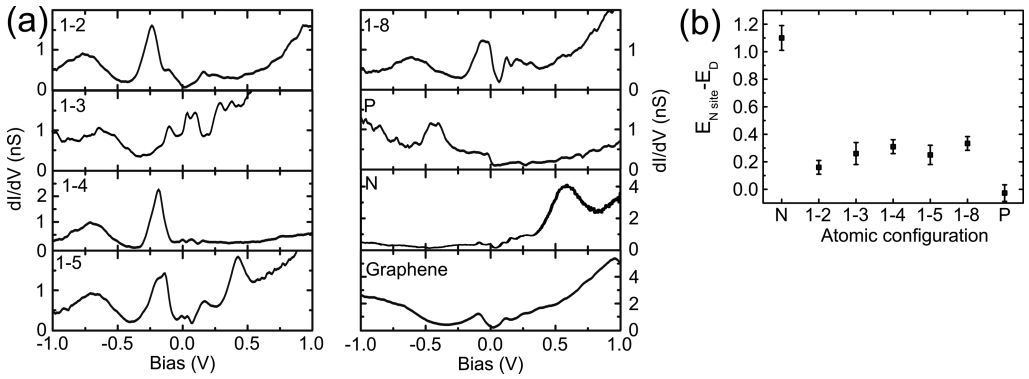

Figure 2. (a) STS measured at the center of different nitrogen pairs. A typical spectrum of a single substitutional nitrogen atom (N) and a spectrum measured on the graphene sheet far from the nitrogen atoms are also shown. To ensure the reliability of the data, all spectra presented here were recorded with calibrated tips, as described in the Methods section. (b) Peak positions of the localized states with respect to the Dirac energy of different nitrogen pair and pyridinic configurations (P) with respect to the Dirac point.

patterns, allowing us to identify them as nitrogen pairs. High-resolution views are shown in Figure 1b, c, d, and e, together with grids indicating the honeycomb lattice. We labeled the pairs as a function of the nitrogen lattice site configuration as depicted in Figure 1g. In this notation the 1−2 pair corresponds to two N atoms in first neighbor position, 1−3 to second neighbors, *etc.*[38] Note that the nitrogen atoms of 1−3, 1−6, and 1−7 pairs are located on the same graphene sublattice, whereas for 1−2, 1−4, 1−5, and 1−8 pairs, the nitrogen atoms occupy both sublattices. An analysis of the frequency of occurrence of each pair, performed for ∼700 defects recorded on nine different images, reveals that the pair distribution follows an intermediate behavior between thermodynamical stability and random distribution; this distribution is disccussed in detail in the Supporting Information. The patterns corresponding to the nitrogen pairs are in most cases the superposition of the two triangular patterns associated with each nitrogen atom. In the zoomed picture in Figure 1b for example, associated with a 1−2 pair, this superposition produces a square-like shape. For the 1−3 pair, a pattern with a central void (Figure 1c) is often observed, in very good agreement with the experimental and theoretical images recently reported by Telychko *et al.*[24] for a metallic tungsten tip. However, another pattern more resembling the expected two-triangle shape can be observed (see Figure 1c), showing again the importance of experimental conditions. For the 1−4 pairs (Figure 1d) the images show a diamond shape that is built on two triangles sharing an edge. The 1−5 pairs (Figure 1a) display a characteristic "dumbbell" shape made of two triangles sharing half of an edge. The typical pattern obtained for 1−8 pairs (Figure 1e) can be described as two triangles separated by a small gap. An additional pattern with a nontrivial shape marked P is also observed (Figure 1a and f): a central dot surrounded by three bars and some extended oscillations of the wave functions. This structure has been observed previously[9] and, as discussed in the theoretical section below, is assigned to a pyridinic configuration. It is to be noted that the oscillations of the wave function, particularly visible for the P configuration in the data presented in Figure 1a, have previously been observed for single N atoms.[8,9] These interference patterns are typical of the interaction between a spatially localized defect state and the delocalized wave functions of graphene.[39]

The apparent height of nitrogen pairs at the bias voltage −0.5 V is higher than that of single substitutional nitrogen (1.0 Å) and depends on the atomic configuration: the apparent heights of 1−2, 1−4, 1−5, and 1−8 pairs are 1.4, 2.0, 1.7, and 1.7 Å, respectively. Since STM probes the local density of states and since no topological effects are expected, the systematically larger height of N pairs compared to single N atoms should be explained by electronic effects. Moreover, contrary to substitutional nitrogen, which exhibits a localized state at positive bias voltage (see Figure 2a and ref 9), and as discussed below, the localized electronic states corresponding to the nitrogen pairs appear brighter at negative bias voltage, explaining the systematically observed larger height.

In order to probe the exact local electronic structure of the complex defects presented in Figure 1a, we performed STS measurements for all structures observed in the STM images. STS spectra recorded for the nitrogen pairs and the pyridinic configuration are reported in Figure 2a, together with a reference spectrum (denoted graphene) taken a few nanometers away from any doping site. This reference plot, typical of N-doped graphene,[8,9] displays two minima: one at the Fermi level (0 eV), which is attributed to the inelastic excitation of a phonon,[2,9] and one at about −0.35 eV, corresponding to the sample's Dirac point. The spectrum of a single substitutional N atom is also presented in Figure 2a (denoted N). In agreement with our previous report,[9] a broad peak centered about 0.6 eV above the Fermi energy (0.95 eV above the Dirac

point) corresponds to an unoccupied state localized around the substitutional N atom and its first carbon neighbors. Regarding the nitrogen pairs, the results reported in Figure 2a show that a peak appears at negative bias, between the Fermi level and the Dirac point, on all the nitrogen pairs. Indeed, we observe a peak at −0.24 V for 1−2, −0.19 V for 1−4, −0.17 V for 1−5, and −0.05 V for the 1−8 configuration. For the 1−3 pair, the spectrum does not show a feature as clear as for the other types of pairs. However, the most systematic feature is a single peak observed at about −0.10 eV. Such localized states were observed for several nitrogen pairs, and the peak positions with respect to the Dirac point are reported in Figure 2b. We attribute the dispersion of the energy positions to environmental effects including the surrounding nitrogen atoms, underlying graphene sheets, and tip state. In addition, the spectroscopy measured on the P configuration shows a broad peak around −0.42 V, close to the Dirac point (−0.35 V). The more systematic measurement reported in Figure 2a shows that the state associated with the P configuration always appears at an energy slightly below the Dirac point. This feature together with the STM image is in good agreement with a pyridinic configuration.[27]

Theoretical Interpretation: Nitrogen Pairs. In order to interpret these experimental results, we have undertaken an investigation of the electronic structure of nitrogen pairs based on *ab initio* and tight-binding calculations. Due to the use of finite supercells, *ab initio* methods are known to suffer from several disadvantages when used for isolated defects and the shape and positions of resonant states.[25] On the other hand since the wave functions are more properly described, they are more accurate locally than the tight-binding method to simulate STM images with different types of atoms.

We first recall the results obtained for a single graphitic N impurity. The local density of states (LDOS) close to the Dirac point on the N atom is shown in Figure 3 (top). To compare TB (Figure 3a) and DFT simulations (Figure 3b), the reference energy has been taken at the Dirac energy. The resonance at about 0.8 eV above the Dirac energy has been observed experimentally[8,9] and largely commented on in detail theoretically.[25] A striking example is also shown in Figure 2a. This LDOS feature is easily explained within a tight-binding approximation with a local potential U on the N site. This extremely simple model is not very accurate quantitatively but very useful to understand trends. Indeed, the local Green function on the N site diverges when $1 - UG^0_{00}(E) = 0$, where $G^0_{00}(E)$ is the local Green function of pristine graphene.[39] Actually since both real and imaginary parts of this quantity do not vanish generally at the same energy, we obtain a resonant state when the real part vanishes, provided the imaginary part remains weak. This happens at weak

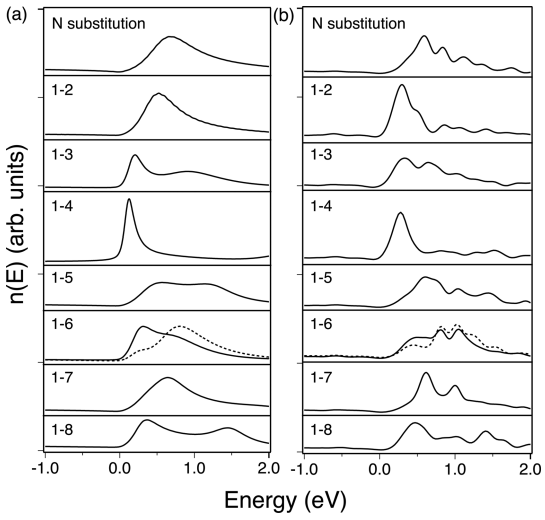

Figure 3. Comparison of the local densities of states on the nitrogen atoms of different pairs calculated with tight-binding model (a) and DFT (b). The origin of the energy is taken at the Dirac point. Note that for the 1−6 pair the two N sites are not equivalent: the continuous line corresponds to site 1 and the dashed one to site 6.

positive energy in the case of an attractive (negative) potential, *i.e.*, for single substitution.[25] The electronic states corresponding to this resonance are mainly localized around the N site.

If we now consider two nearby impurities, their resonant states are coupled through the lattice, and this gives rise to bonding and antibonding states. Mathematically they are obtained from the vanishing of a 2×2 determinant involving the matrix elements of the full Green operator on both sites.[40] However, the upper resonance occurs at energies where the graphene density of states is fairly high, so it is actually washed out. The lower (bonding) resonance on the other hand moves toward the Dirac point and sharpens. Simple calculations predict that it can even cross the Dirac point.[41] Using a more realistic tight-binding model with potentials extended to the first neighbors,[25] we have calculated the local densities of states for different nitrogen pairs. We assumed, for nearby dopants, that we can superimpose the potentials of the isolated impurities, which is reasonable except for the first neighbor pair, where the procedure is obviously problematic. In this case we have not superimposed the potentials on the N atoms. The results are shown in Figure 3a and compared with the DFT data obtained for a (10×10) (200 atoms) supercell in Figure 3b. The very good agreement between both approaches justifies the above assumption for the TB. The oscillations in the densities of the DFT simulations are related to the interference effect and to the finite size of the supercell.[25] The general trend is consistent with our simple analysis above. The resonance moves toward the Dirac point, but remains above it, and it is especially well defined for the third neighbor pair ("para" 1−4 configuration). This is in very good semiquantitative

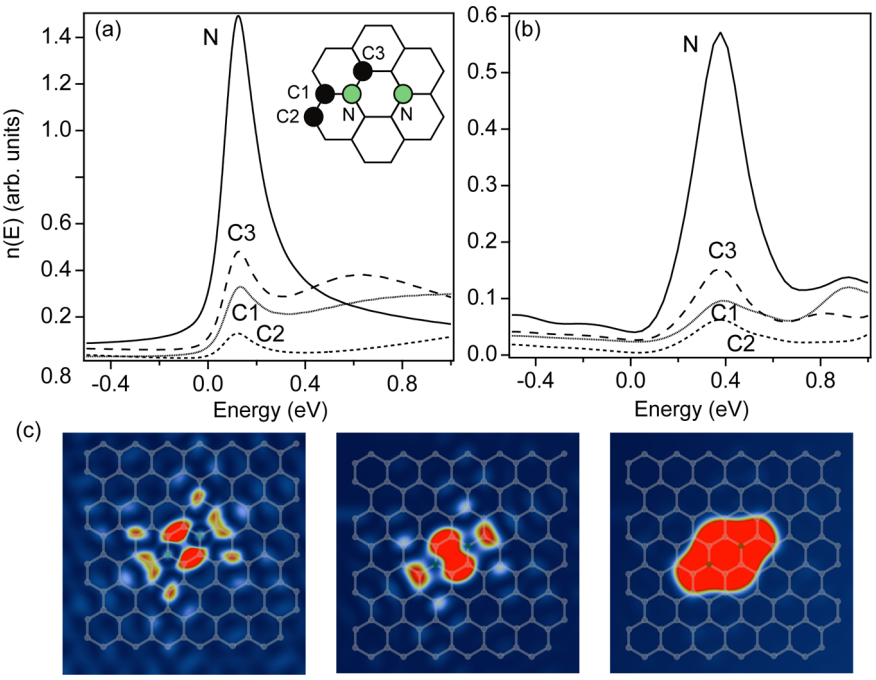

Figure 4. Tight-binding (a) and DFT (b) local densities of states on the nitrogen atom and carbon atoms around a third-neighbor nitrogen pair (1−4). (c) Corresponding DFT-based STM image obtained within the Tersoff−Hamann approach at 2, 3, and 5 Å (from left to right) above the atomic plane and for a bias of −0.5 V.

agreement with experiment, where the resonance occurs below the Fermi level but a few tenths of an eV above the Dirac point. Direct comparison with experimental STS (Figure 2) is difficult because of the drop of the spectra at the Fermi level (see above). However, experimental data and simulations agree fairly well for the 1−2 and 1−4 pairs. In terms of doping, the observation of resonances above the Dirac point suggests that the presence of nitrogen pairs would result in n-type doped graphene, in the absence of other configurations. This is in agreement with the data reported by Lv *et al.* for 1−3 pairs.[18]

In order to analyze STM images, we have also calculated the LDOS on several carbon sites near the nitrogen pairs. In Figure 4a and b, we display the TB and DFT calculations of the local density on the N atoms and on the neighboring C atoms for the 1−4 pair. Both approaches are in good agreement and reveal a resonance on the N site larger than on the neighboring C atoms. The corresponding peak coincides here with those observed for the C1, C2, and C3 atoms. Moreover, Figure 4 reveals that there are much fewer electronic states in the region between 0 and 0.4 eV on the second-neighbor atoms (C2) than on the third- (C3) and first-neighbor (C1) carbons. In Figure 4c, the computed STM images, obtained within the Tersoff−Hamann approach at different heights (2 to 5 Å) above the atomic plane and for a bias of −0.5 V, are presented. The reference energy is at the Dirac point, and the Fermi energy obtained in DFT is at 0.44 eV. The electron states considered for the STM image are then between −0.06 and +0.44 eV. At 2 Å, N atoms are not imaged despite the large LDOS on that site. This is related to the very fast decrease of the p_z wave function of positively charged N atoms.[27] Simulations performed for an unrealistic short tip−sample distance (1 Å) display bright features on N atoms (not shown).

In Figure 4c, the images computed at 3 and 5 Å have been obtained with an analytical prolongation of the DFT wave function and reveal the tip−sample distance dependence of the STM images. Indeed, the tip−sample distance selects the wave function as a function of the exponential decrease of the p_z orbitals associated with N atoms or C atoms with different local charge transfer. The lateral extension of the "atomic" wave function also increases with the distance from the atomic surface. Both effects combine and produce the variation observed in Figure 4c. The theoretical image calculated at 5 Å is in good agreement with the experimental image presented in Figure 1d. STM series on the same defect and with the same tip (see Joucken *et al.*[9]) confirm that such an effect is indeed observed. Similar fingerprints have also been attributed to a tip composition effect.[24]

In Figure 5 are presented simulated STM images computed at 5 Å above the graphene layers for two other nitrogen pairs (1−2 and 1−8). Like the example of the 1−4 pair displayed in Figure 4c, these calculated images are in good agreement with the experimental images displayed in Figure 1b and e.

Theoretical Interpretation: Pyridinic Configurations. Let us now consider the so-called pyridinic configuration. Its experimental signature, a triangular shape in the STM image and a peak appearing at −0.42 V just below the

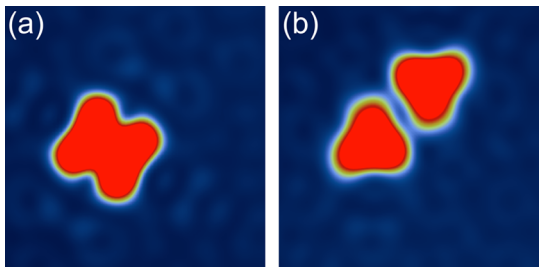

Figure 5. DFT-based computed STM images of a nitrogen-doped graphene showing nitrogen pairs at 5 Å above the atomic plane: (a) 1−2 pair; (b) 1−8 pair.

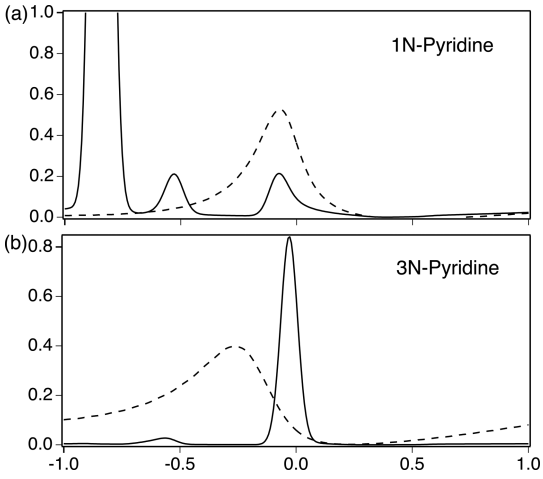

Figure 6. Local densities of states on the nitrogen atom of the 1N- (a) and 3N-pyridine; (b) configurations showing a strong resonance just below the Dirac point. Full line: DFT calculations; dashed line: TB calculations. The sharp peak at low energy in the DFT calculation for the 1N-pyridine is due to a σ state, whereas the splitting of the resonance is induced by a supercell effect.

Dirac energy in STS, is different from that of the N pairs. Besides substitutional N atoms, the presence of pyridine defects, where a vacancy is combined with one or several nitrogen neighboring atoms, has been evidenced by X-ray absorption and photoelectron spectroscopies for both N-doped graphene[42] and N-doped graphite.[43] Using theoretical calculations, the most studied configurations are the monomeric (1N-pyridine) or trimerized (3N-pyridine) pyridine-type defects.[17,18,20,23,27,38,43−45] It is generally found theoretically that STS spectra display a resonance below the Dirac point, indicating that graphene functionalized with pyridine groups would be only p-doped. In terms of STM simulations, the calculated images show typical shapes with three arms starting from the vacancy site. Previous experimental STM observations are scarce; the images recorded by Kondo *et al.*[43] on the surface of N-doped graphite are associated with 1N-pyridine.

To better understand such defects, we present in Figure 6 electronic structure calculations based on *ab initio* and tight-binding calculations. LDOS can be understood from simple tight-binding arguments. Consider a 1N configuration and introduce a vacancy.

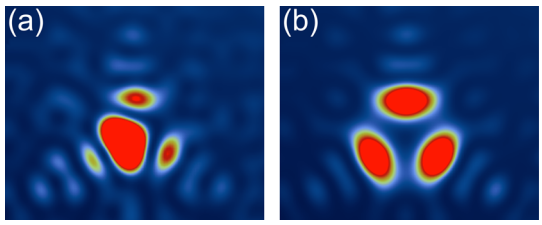

Figure 7. DFT-based STM images. Calculations with the Tersoff−Hamman approach at 5 Å above the atomic plane for 1N-pyridine (a) and 3N-pyridine (b).

It is well known that the vacancy induces a strong resonance at the Dirac point with divergent behaviors of the LDOS (for a review, see ref 39). This concerns the π states, but in this case we also have to look at the broken bond and, consequently, at the corresponding σ states. It turns out that *ab initio* calculations show that they form bound states below the Dirac point.[17,45] Then there is an additional occupied σ state, and the effective potential of the nitrogen impurity is partially screened and much weaker than for a substitutional impurity. Finally, this potential acting on the vacancy resonant state simply lowers its energy below the Dirac point. This is exactly what we find using reduced values for the potentials $U_1 = -1$ eV and $U_2 = -0.5$ eV on the nitrogen atom and its neighbors, respectively, as shown in Figure 6. Calculations for a 3N-pyridine configuration are actually very similar. Theoretical STM images of 1N-pyridine and 3N-pyridine are presented in Figure 7. In the case of the 1N pyridine, a central triangle is surrounded by three arms, the symmetry is low, and small local relaxations should be introduced as for the vacancy.[46] In the latter case the two carbon atoms near the vacancy close a pentagon by forming a new σ bond, and this modifies slightly the energy of the resonance, but the calculated images show that the lowering of symmetry should be hardly visible. The calculated image for the 3N-pyridine is more symmetrical, but there is no central triangle. Thus, the observed defect presents a clear signature of a vacancy-like defect, but there is no obvious way to decide whether the observed defect P is a 1N- or 3N-pyridine defect even if the 1N configuration seems more plausible. The red dots in Figure 1f mark the three possible positions for the pyridinic N atom (all three positions are occupied in the case of a 3N-pyridine).

CONCLUSION

In this work, we have shown that different configurations of nitrogen impurities can be clearly identified by comparing STM-STS observations with electronic structure calculations. To summarize, single graphitic N atoms are imaged as typical triangles and induce resonances in the LDOS at positive energies (about 0.95 eV above the Dirac energy in the STS spectra and 0.8 eV for the calculated DOS). Nitrogen pairs are imaged as superposition of triangles with, in some

cases, interference effects. TB and DFT simulations allow us to catch the main features of the STM images and STS spectra. Further evidence is the good agreement between the experimental STM images for the most common complex N-doped systems (Figure 1) and the DFT counterparts (Figure 4, Figure 5). The single impurity resonance is then replaced by a bonding resonance at lower energy, a few tenths of an eV above the Dirac point. Finally pyridinic configurations produce other typical triangular images with bars transversal to triangular arms. The resonance here occurs at slightly negative energies below the Dirac point. It has frequently been argued that this is consistent with an n-type (donor) character of graphitic N atoms and a p-type (acceptor) character of pyridinic configurations.[17] Graphitic N atoms provide electrons to the conduction band, and this is clearly seen in photoemission experiments,[20,42] STS,[9] and *ab initio* calculations.[25,45] In our experiments, the Fermi energy is about 0.4 eV above the Dirac point for a fairly high concentration of dopants (~1.3%). Conversely, there is evidence that in the case of pyridine configurations alone the Fermi level should move in the valence band and p-doping occurs. This does not happen in our case because the concentration of graphitic N atoms is predominant. We are in a situation of a globally heavily doped, compensated n-type semiconductor. At very low concentration, on the other hand, behaviors more typical of a genuine semiconductor are expected. Even if global doping depends on defect concentrations and on the doping process, our local STM/STS study provides a detailed background to better understand the electronic properties of chemically doped graphene.

METHODS

The graphene samples were prepared from C-terminated n-type 6H-SiC(000$\bar{1}$) wafers, following procedures available in the literature;[28,47−50] the details of our growth method have been published previously.[9] As extensively discussed in the literature, the multilayer graphene obtained on this substrate mostly consists of rotationally disordered graphene domains that are effectively decoupled.[28−35] N-doping was achieved by exposing the samples to an atomic nitrogen flux produced by a remote radiofrequency plasma source fed with N_2. The plasma generator is not in the close vicinity of the sample in order to reduce the number of possible interactions between the nitrogen source and the pristine graphene. Thus, only the topmost layer is affected by the plasma treatment. The samples were then transferred in air to a low-temperature STM apparatus (Omicron) working at 5 K and at a pressure lower than 1×10^{-11} mbar and degassed at about 900 °C for 1 h before the measurements. Differential conductance spectra were obtained using a lock-in amplifier with a modulation at about 600 Hz and 50 mV. The STM tips used in this study were electrochemically etched tungsten tips. As shown in the literature,[2,24] reliable STM and STS experiments on graphene require the use of properly metallized tips. Therefore, we used a procedure that consists in applying bias positive and negative pulses (up to ±10 V) between the tip and a Au(111) surface until the STS spectra obtained for Au(111) displayed the gold surface state at −0.4 V while still retaining a good spatial resolution. Such gold-prepared tips were considered as calibrated[2] and could be used for STM and STS of N-doped graphene (showing triangular shapes for graphitic N atoms and STS spectra of graphene similar to that of Figure 2a (bottom-right panel)) during a few hours before contamination, probably by carbon. The preparation procedure was followed again to regenerate the tip. It is to be noted that we used data recorded on the same sample in Figure 1 and Figure 2, although the same experimental signatures were observed for several samples.

All tight-binding and DFT calculations have been performed for monolayer graphene. The tight-binding method is based on the usual description of the π states of graphene with a single transfer integral t between first neighbors equal to 2.72 eV. The potential due to the nitrogen impurity is assumed to reduce to on-site energies on the nitrogen site and its first neighbors. They have been determined so as to fit at best *ab initio* calculations and are equal to $U_1 = -4$ eV and $U_2 = -2.57$ eV, respectively. The local densities of states projected on lattice sites $n_{nn}(E)$ are calculated using the recursion method.[25] Spatial LDOS are calculated from $n(\vec{r}, E) = \sum_{n,m} n_{n,m}(E)\, \phi(\vec{r} - \vec{n})\, \phi(\vec{r} - \vec{m})$, where $\phi(\vec{r})$ is a π orbital. In practice to mimic an image at some height, we just replace it by a two-dimensional s-like orbital.

The *ab initio* electronic structure simulations have been performed within the density functional theory as implemented in the SIESTA package.[51] A supercell technique (10×10 unit cell including 198 C atoms and two N atoms) was used to investigate N-doped graphene. A vacuum region of about 10 Å between the layers has been taken in order to avoid undesired interactions between periodically repeated images along the direction perpendicular to the sheets. Exchange−correlation effects were handled within the local density approximation as proposed by Perdew and Zunger.[52] Core electrons were replaced by nonlocal norm-conserving pseudopotentials.[53] The valence electrons were described by localized pseudoatomic orbitals with a double-ζ for the substitution and a double-ζ with polarization for pyridine-like systems.[54] For the self-consistent electronic density calculations, the first Brillouin zone was sampled with a $15 \times 15 \times 1$ grid generated according to the Monkhorst−Pack scheme[55] in order to ensure a good convergence. Real-space integration was performed on a regular grid corresponding to a plane-wave cutoff around 200 Ry. All the atomic structures of self-supported doped graphene have been relaxed (with fixed lattice parameters for the supercell) using a conjugate gradient scheme until the maximum residual forces on each atom were smaller than 0.01 eV/Å. The STM topological images at 2 Å for the graphene plane were calculated according to the Tersoff and Hamann approximation, following the methodology applied before.[27,56] STM images at higher distance were obtained by an analytical prolongation of the wave function as implemented in the STM package of the SIESTA code.

Conflict of Interest: The authors declare no competing financial interest.

Acknowledgment. V.R. thanks the Institut Universitaire de France for support. Y.T. thanks the Labex SEAM program No. ANR-11-LABX-086 for financial support in the framework of the Program No. ANR-11-IDEX-0005-02. The research leading to these results has received funding from the European Union Seventh Framework Programme under grant agreement no. 604391 Graphene Flagship. This research used resources of the "Plateforme Technologique de Calcul Intensif (PTCI)" (http://www.ptci.unamur.be) located at the University of Namur, Belgium, which is supported by the F.R.S.-FNRS under the convention no. 2.4520.11. The PTCI is a member of the "Consortium des Équipements de Calcul Intensif (CÉCI)" (http://www.ceci-hpc.be). D.S. is supported by the UNamur-CERUNA program.

Supporting Information Available: An analysis of the frequency of occurrence of each pair, schematic pictures of the

different defects involving N atoms, the corresponding local densities of state calculated within the tight-binding approximation, and maps of the local densities of state integrated in a 0.5 eV window around the resonance are provided. This material is available free of charge *via* the Internet at http://pubs.acs.org.

REFERENCES AND NOTES

1. Lv, R.; Terrones, M. Towards New Graphene Materials: Doped Graphene Sheets and Nanoribbons. *Mater. Lett.* **2012**, *78*, 209–218.
2. Zhang, Y.; Brar, V. W.; Wang, F.; Girit, C.; Yayon, Y.; Panlasigui, M.; Zettl, A.; Crommie, M. F. Giant Phonon-Induced Conductance in Scanning Tunnelling Spectroscopy of Gate-Tunable Graphene. *Nat. Phys.* **2008**, *4*, 627–630.
3. Zhou, S. Y.; Siegel, D. A.; Fedorov, A. V.; Lanzara, A. Metal to Insulator Transition in Epitaxial Graphene Induced by Molecular Doping. *Phys. Rev. Lett.* **2008**, *101*, 086402.
4. Kaverzin, A.; Strawbridge, S.; Price, A.; Withers, F.; Savchenko, A.; Horsell, D. Electrochemical Doping of Graphene with Toluene. *Carbon* **2011**, *49*, 3829–3834.
5. Zhang, W.; Lin, C.-T.; Liu, K.-K.; Tite, T.; Su, C.-Y.; Chang, C.-H.; Lee, Y.-H.; Chu, C.-W.; Wei, K.-H.; Kuo, J.-L.; *et al*. Opening an Electrical Band Gap of Bilayer Graphene with Molecular Doping. *ACS Nano* **2011**, *5*, 7517–7524.
6. Panchakarla, L. S.; Subrahmanyam, K. S.; Saha, S. K.; Govindaraj, A.; Krishnamurthy, H. R.; Waghmare, U. V.; Rao, C. N. R. Synthesis, Structure, and Properties of Boron- and Nitrogen-Doped Graphene. *Adv. Mater. (Weinheim, Ger.)* **2009**, *21*, 4726–4730.
7. Wang, H.; Maiyalagan, T.; Wang, X. Review on Recent Progress in Nitrogen-Doped Graphene: Synthesis, Characterization, and Its Potential Applications. *ACS Catal.* **2012**, *2*, 781–794.
8. Zhao, L.; He, R.; Rim, K. T.; Schiros, T.; Kim, K. S.; Zhou, H.; Gutiérrez, C.; Chockalingam, S. P.; Arguello, C. J.; Pálová, L.; *et al*. Visualizing Individual Nitrogen Dopants in Monolayer Graphene. *Science* **2011**, *333*, 999–1003.
9. Joucken, F.; Tison, Y.; Lagoute, J.; Dumont, J.; Cabosart, D.; Zheng, B.; Repain, V.; Chacon, C.; Girard, Y.; Botello-Méndez, A. R.; *et al*. Localized State and Charge Transfer in Nitrogen-Doped Graphene. *Phys. Rev. B: Condens. Matter Mater. Phys.* **2012**, *85*, 161408.
10. Zhao, L.; Levendorf, M.; Goncher, S.; Schiros, T.; Pálová, L.; Zabet-Khosousi, A.; Rim, K. T.; Gutiérrez, C.; Nordlund, D.; Jaye, C.; *et al*. Local Atomic and Electronic Structure of Boron Chemical Doping in Monolayer Graphene. *Nano Lett.* **2013**, *13*, 4659–4665.
11. Zabet-Khosousi, A.; Zhao, L.; Pálová, L.; Hybertsen, M. S.; Reichman, D. R.; Pasupathy, A. N.; Flynn, G. W. Segregation of Sublattice Domains in Nitrogen-Doped Graphene. *J. Am. Chem. Soc.* **2014**, *136*, 1391–1397.
12. Chang, D. W.; Lee, E. K.; Park, E. Y.; Yu, H.; Choi, H.-J.; Jeon, I.-Y.; Sohn, G.-J.; Shin, D.; Park, N.; Oh, J. H.; *et al*. Nitrogen-Doped Graphene Nanoplatelets from Simple Solution Edge-Functionalization for n-Type Field-Effect Transistors. *J. Am. Chem. Soc.* **2013**, *135*, 8981–8988.
13. Ghosh, A.; Late, D. J.; Panchakarla, L. S.; Govindaraj, A.; Rao, C. N. R. NO_2 and Humidity Sensing Characteristics of Few-Layer Graphenes. *J. Exp. Nanosci.* **2009**, *4*, 313–322.
14. He, C.; Wang, R.; Fu, H.; Shen, P. K. Nitrogen-Self-Doped Graphene as a High Capacity Anode Material for Lithium-Ion Batteries. *J. Mater. Chem. A* **2013**, *1*, 14586–14591.
15. Deng, D.; Pan, X.; Yu, L.; Cui, Y.; Jiang, Y.; Qi, J.; Li, W.-X.; Fu, Q.; Ma, X.; Xue, Q.; *et al*. Toward N-Doped Graphene via Solvothermal Synthesis. *Chem. Mater.* **2011**, *23*, 1188–1193.
16. Huang, C.; Li, C.; Shi, G. Graphene Based Catalysts. *Energy Environ. Sci.* **2012**, *5*, 8848–8868.
17. Schiros, T.; Nordlund, D.; Pálová, L.; Prezzi, D.; Zhao, L.; Kim, K. S.; Wurstbauer, U.; Gutiérrez, C.; Delongchamp, D.; Jaye, C.; *et al*. Connecting Dopant Bond Type with Electronic Structure in N-Doped Graphene. *Nano Lett.* **2012**, *12*, 4025–4031.
18. Lv, R.; Li, Q.; Botello-Méndez, A. R.; Hayashi, T.; Wang, B.; Berkdemir, A.; Hao, Q.; Elías, A. L.; Cruz-Silva, R.; Gutiérrez, H. R.; *et al*. Nitrogen-Doped Graphene: Beyond Single Substitution and Enhanced Molecular Sensing. *Sci. Rep.* **2012**, *2*, 586.
19. Guo, B.; Liu, Q.; Chen, E.; Zhu, H.; Fang, L.; Gong, J. R. Controllable N-Doping of Graphene. *Nano Lett.* **2010**, *10*, 4975–4980.
20. Usachov, D.; Vilkov, O.; Grüneis, A.; Haberer, D.; Fedorov, A.; Adamchuk, V. K.; Preobrajenski, A. B.; Dudin, P.; Barinov, A.; Oehzelt, M.; *et al*. Nitrogen-Doped Graphene: Efficient Growth, Structure, and Electronic Properties. *Nano Lett.* **2011**, *11*, 5401–5407.
21. Wang, H.; Wang, Q.; Cheng, Y.; Li, K.; Yao, Y.; Zhang, Q.; Dong, C.; Wang, P.; Schwingenschlögl, U.; Yang, W.; *et al*. Doping Monolayer Graphene with Single Atom Substitutions. *Nano Lett.* **2012**, *12*, 141–144.
22. Koch, R. J.; Weser, M.; Zhao, W.; Viñes, F.; Gotterbarm, K.; Kozlov, S. M.; Höfert, O.; Ostler, M.; Papp, C.; Gebhardt, J.; *et al*. Growth and Electronic Structure of Nitrogen-Doped Graphene on Ni(111). *Phys. Rev. B: Condens. Matter Mater. Phys.* **2012**, *86*, 075401.
23. Usachov, D.; Fedorov, A.; Vilkov, O.; Senkovskiy, B.; Adamchuk, V. K.; Yashina, L. V.; Volykhov, A. A.; Farjam, M.; Verbitskiy, N. I.; Grüneis, A.; *et al*. The Chemistry of Imperfections in N-Graphene. *Nano Lett.* **2014**, *14*, 4982–4988.
24. Telychko, M.; Mutombo, P.; Ondráček, M.; Hapala, P.; Bocquet, F. C.; Kolorenč, J.; Vondráček, M.; Jelínek, P.; Švec, M. Achieving High-Quality Single-Atom Nitrogen Doping of Graphene/SiC(0001) by Ion Implantation and Subsequent Thermal Stabilization. *ACS Nano* **2014**, *8*, 7318–7324.
25. Lambin, P.; Amara, H.; Ducastelle, F.; Henrard, L. Long-Range Interactions between Substitutional Nitrogen Dopants in Graphene: Electronic Properties Calculations. *Phys. Rev. B: Condens. Matter Mater. Phys.* **2012**, *86*, 045448.
26. Adjizian, J.-J.; Leghrib, R.; Koos, A. A.; Suarez-Martinez, I.; Crossley, A.; Wagner, P.; Grobert, N.; Llobet, E.; Ewels, C. P. Boron- and Nitrogen-Doped Multi-Wall Carbon Nanotubes for Gas Detection. *Carbon* **2014**, *66*, 662–673.
27. Zheng, B.; Hermet, P.; Henrard, L. STM Simulations of Nitrogen and Boron Doped Graphene and Single-Walled Carbon Nanotubes. *ACS Nano* **2010**, *7*, 4165.
28. Varchon, F.; Mallet, P.; Magaud, L.; Veuillen, J.-Y. Rotational Disorder in Few-Layer Graphene Films on 6H-SiC(000−1): A Scanning Tunneling Microscopy Study. *Phys. Rev. B: Condens. Matter Mater. Phys.* **2008**, *77*, 165415.
29. Hass, J.; Varchon, F.; Millan-Otoya, J. E.; Sprinkle, M.; Sharma, N.; de Heer, W. A.; Berger, C.; First, P. N.; Magaud, L.; Conrad, E. H. Why Multilayer Graphene Grown on the SiC(000−1) C-Face Behaves Like a Single Sheet of Graphene. *Phys. Rev. Lett.* **2008**, *100*, 125504.
30. Biedermann, L. B.; Bolen, M. L.; Capano, M. A.; Zemlyanov, D.; Reifenberger, R. G. Insights into Few-Layer Epitaxial Graphene Growth on 4H-SiC(000$\bar{1}$) Substrates from STM Studies. *Phys. Rev. B: Condens. Matter Mater. Phys.* **2009**, *79*, 125411.
31. Miller, D. L.; Kubista, K. D.; Rutter, G. M.; Ruan, M.; de Heer, W. A.; First, P. N.; Stroscio, J. A. Observing the Quantization of Zero Mass Carriers in Graphene. *Science* **2009**, *324*, 924–927.
32. Sprinkle, M.; Siegel, D.; Hu, Y.; Hicks, J.; Tejeda, A.; Taleb-Ibrahimi, A.; Le Fèvre, P.; Bertran, F.; Vizzini, S.; Enriquez, H.; *et al*. First Direct Observation of a Nearly Ideal Graphene Band Structure. *Phys. Rev. Lett.* **2009**, *103*, 226803.
33. Sprinkle, M.; Hicks, J.; Tejeda, A.; Taleb-Ibrahimi, A.; Le Fèvre, P.; Bertran, F.; Tinkey, H.; Clark, M. C.; Soukiassian, P.; Martinotti, D.; *et al*. Multilayer Epitaxial Graphene Grown on the SiC(000−1) Surface; Structure and Electronic Properties. *J. Phys. D: Appl. Phys.* **2010**, *43*, 374006.
34. Miller, D. L.; Kubista, K. D.; Rutter, G. M.; Ruan, M.; de Heer, W. A.; First, P. N.; Stroscio, J. A. Structural Analysis of Multilayer Graphene via Atomic Moiré Interferometry. *Phys. Rev. B: Condens. Matter Mater. Phys.* **2010**, *81*, 125427.
35. Brihuega, I.; Mallet, P.; González-Herrero, H.; Trambly de Laissardiére, G.; Ugeda, M. M.; Magaud, L.; Gómez-Rodríguez, J. M.; Ynduráin, F.; Veuillen, J.-Y. Unraveling the Intrinsic and Robust Nature of van Hove Singularities

in Twisted Bilayer Graphene by Scanning Tunneling Microscopy and Theoretical Analysis. *Phys. Rev. Lett.* **2012**, *109*, 196802.
36. Tison, Y.; Lagoute, J.; Repain, V.; Chacon, C.; Girard, Y.; Joucken, F.; Sporken, R.; Gargiulo, F.; Yazyev, O. V.; Rousset, S. Grain Boundaries in Graphene on SiC(000$\bar{1}$) Substrate. *Nano Lett.* **2014**, *14*, 6382–6386.
37. Lherbier, A.; Botello-Mendez, A. R.; Charlier, J.-C. Electronic and Transport Properties of Unbalanced Sublattice N-Doping in Graphene. *Nano Lett.* **2013**, *13*, 1446–1450.
38. Hou, Z.; Wang, X.; Ikeda, T.; Terakura, K.; Oshima, M.; Kakimoto, M.-a.; Miyata, S. Interplay Between Nitrogen Dopants and Native Point Defects in Graphene. *Phys. Rev. B: Condens. Matter Mater. Phys.* **2012**, *85*, 165439.
39. Ducastelle, F. Electronic Structure of Vacancy Resonant States in Graphene: A Critical Review of the Single-Vacancy Case. *Phys. Rev. B: Condens. Matter Mater. Phys.* **2013**, *88*, 075413.
40. Lifshitz, I. Energy Spectrum Structure and Quantum States of Disordered Condensed Systems. *Sov. Phys. Usp.* **1965**, *7*, 549–573.
41. Wehling, T. O.; Balatsky, A. V.; Katsnelson, M. I.; Lichtenstein, A. I.; Scharnberg, K.; Wiesendanger, R. Local Electronic Signatures of Impurity States in Graphene. *Phys. Rev. B: Condens. Matter Mater. Phys.* **2007**, *75*, 125425.
42. Velez-Fort, E.; Mathieu, C.; Pallecchi, E.; Pigneur, M.; Silly, M. G.; Belkhou, R.; Marangolo, M.; Shukla, A.; Sirotti, F.; Ouerghi, A. Epitaxial Graphene on 4H-SiC(0001) Grown under Nitrogen Flux: Evidence of Low Nitrogen Doping and High Charge Transfer. *ACS Nano* **2012**, *6*, 10893–10900.
43. Kondo, T.; Casolo, S.; Suzuki, T.; Shikano, T.; Sakurai, M.; Harada, Y.; Saito, M.; Oshima, M.; Trioni, M. I.; Tantardini, G. F.; *et al*. Atomic-Scale Characterization of Nitrogen-Doped Graphite: Effects of Dopant Nitrogen on the Local Electronic Structure of the Surrounding Carbon Atoms. *Phys. Rev. B: Condens. Matter Mater. Phys.* **2012**, *86*, 035436.
44. Fujimoto, Y.; Saito, S. Formation, Stabilities, and Electronic Properties of Nitrogen Defects in Graphene. *Phys. Rev. B: Condens. Matter Mater. Phys.* **2011**, *84*, 245446.
45. Hou, Z.; Wang, X.; Ikeda, T.; Terakura, K.; Oshima, M.; Kakimoto, M. Electronic Structure of N-Doped Graphene with Native Point Defects. *Phys. Rev. B: Condens. Matter Mater. Phys.* **2013**, *87*, 165401.
46. Amara, H.; Latil, S.; Meunier, V.; Lambin, P.; Charlier, J.-C. Scanning Tunneling Microscopy Fingerprints of Point Defects in Graphene: A Theoretical Prediction. *Phys. Rev. B: Condens. Matter Mater. Phys.* **2007**, *76*, 115423.
47. Forbeaux, I.; Themlin, J.-M.; Debever, J.-M. High-Temperature Graphitization of the 6H-SiC (0001) Face. *Surf. Sci.* **1999**, *442*, 9.
48. de Heer, W. A.; Berger, C.; Wu, X.; First, P. N.; Conrad, E. H.; Li, X.; Li, T.; Sprinkle, M.; Hass, J.; Sadowski, M. L.; *et al*. Epitaxial Graphene. *Solid State Commun.* **2007**, *143*, 92.
49. Hiebel, F.; Mallet, P.; Varchon, F.; Magaud, L.; Veuillen, J.-Y. Graphene-Substrate Interaction on 6H-SiC(000−1): A Scanning Tunneling Microscopy Study. *Phys. Rev. B: Condens. Matter Mater. Phys.* **2008**, *78*, 153412.
50. Starke, U.; Riedl, C. Epitaxial Graphene on SiC(0001) and SiC(000−1): From Surface Reconstructions to Carbon Electronics. *J. Phys.: Condens. Matter* **2009**, *21*, 134016.
51. Sánchez-Portal, D.; Ordejón, P.; Artacho, E.; Soler, J. M. Density-Functional Method for Very Large Systems with LCAO Basis Sets. *Int. J. Quantum Chem.* **1997**, *65*, 453–461.
52. Perdew, J. P.; Zunger, A. Self-Interaction Correction to Density-Functional Approximations for Many-Electron Systems. *Phys. Rev. B: Condens. Matter Mater. Phys.* **1981**, *23*, 5048–5079.
53. Troullier, N.; Martins, J. L. Efficient Pseudopotentials for Plane-Wave Calculations. *Phys. Rev. B: Condens. Matter Mater. Phys.* **1991**, *43*, 1993–2006.
54. Artacho, E.; Sánchez-Portal, D.; Ordejón, P.; García, A.; Soler, J. M. Linear-Scaling ab-Initio Calculations for Large and Complex Systems. *Phys. Status Solidi B* **1999**, *215*, 809–817.
55. Monkhorst, H. J.; Pack, J. D. Special Points for Brillouin-Zone Integrations. *Phys. Rev. B: Solid State* **1976**, *13*, 5188–5192.
56. Tersoff, J.; Hamann, D. R. Theory and Application for the Scanning Tunneling Microscope. *Phys. Rev. Lett.* **1983**, *50*, 1998–2001.